Decay of ^{160}Er* in ^{16}O + ^{144}Nd and ^{64}Ni + ^{96}Zr fusion reactions

J.L. Barreto,* N.G. Nicolis,† D.G. Sarantites, R.J. Charity, L.G. Sobotka, and D.W. Stracener
Department of Chemistry, Washington University, St. Louis, Missouri 63130

D.C. Hensley, J.R. Beene, C. Baktash, M.L. Halbert, and M. Thoennessen‡
Oak Ridge National Laboratory, Oak Ridge, Tennessee 37831
(Received 31 October 1994)

The population of evaporation residue entry states in the decay of the compound nucleus ^{160}Er*(54 MeV) is investigated in a cross-bombardment employing the reactions ^{16}O + ^{144}Nd and ^{64}Ni + ^{96}Zr. Evaporation residue cross sections and entry state γ-ray fold distributions of the dominant exit channels were obtained for each reaction, using a 4π γ-ray detection system. An entrance-channel dependence of the γ-ray fold distributions of the xn products is observed. This effect is described successfully by the statistical model making use of compound nucleus angular momentum distributions obtained with a fusion model that provides a good description of the bombarding energy dependence of fusion data for both reactions. In accordance with recent findings on the decay of ^{164}Yb*, it is suggested that the observed differences in the population of the dominant exit channels originate from the primary spin distributions rather than a possible dependence of the compound nucleus decay on the formation mode.

PACS number(s): 25.70.Gh, 25.70.Jj, 24.60.Dr

I. INTRODUCTION

The formation and decay of compound nuclei have always been of considerable interest in the study of heavy-ion reactions. In the near and below Coulomb barrier energy regime, the fusion cross sections ($\sigma_{\rm fus}$) of many reaction systems have long been known to exhibit an enhancement over the predictions of one-dimensional barrier penetration models [1]. The advent of multidetector γ-ray detection systems made possible measurements of the evaporation residue spin distributions. In a few cases, the difficult task of the compound nucleus angular momentum distribution (σ_ℓ) reconstruction has been undertaken. Such measurements have indicated a broadening of the σ_ℓ distributions accompanying the subbarrier fusion cross-section enhancements. Simultaneous measurements of $\sigma_{\rm fus}$ and σ_ℓ provide valuable information on the fusion process and a stringent test of the fusion models [2,3].

In the rare earth region, certain studies have addressed the role of entrance-channel mass asymmetry on the population of the compound nucleus angular momentum [4–11]. For example, in the work of Haas *et al.* [5] the compound nucleus ^{160}Er* was produced via four reactions of considerably different mass asymmetries at common excitation energies. A dramatic entrance-channel dependence of the average evaporation residue γ-ray multiplicities was observed. The results were interpreted in terms of zero-point vibrations and the implied σ_ℓ distributions were found sufficient to account for the evaporation residue yields and average γ-ray multiplicities calculated with the statistical model. The origin of these effects was also explained with simplified coupled-channels calculations [6]. Another interesting result has been reported by Ruckelshausen *et al.* [10] on the decay of ^{156}Er*(47 MeV) formed in the reactions ^{12}C + ^{144}Sm and ^{64}Ni + ^{92}Zr. Strong differences in the αxn and high-spin xn populations were observed. Furthermore, a reconstruction of the (primary) σ_ℓ distributions indicated an entrance-channel dependence of the ratio of the $2n/3n$ cross sections as a function of the compound nucleus spin. This suggested that there may be memory during the particle evaporation process, in contrast to the Bohr hypothesis concerning the independence of compound nucleus decay on the formation mode.

Motivated by the previous results, Barreto *et al.* [11] studied the deexcitation of ^{164}Yb*(54 MeV) formed in the reactions ^{16}O + ^{148}Sm and ^{64}Ni + ^{100}Mo. Evaporation residue γ-ray fold distributions (k_γ) as well as energy and angular distributions of the emitted light charged particles were observed using 4π multidetector systems. A projectile breakup mechanism in the ^{16}O-induced reaction was found responsible for differences in the k_γ distributions observed in the αxn products of these reactions. Furthermore, the γ-ray fold distributions of the xn products were found consistent with the predictions of the statistical model using σ_ℓ distributions that describe closely measured fusion excitation functions for these systems. It was also pointed out that the shapes of the σ_ℓ distributions play a prominent role in the evaporation yields,

*On leave from Instituto de Física da Universidade Federal do Rio de Janeiro, Caixa Postal, 21945, Rio de Janeiro, Brazil.
†Present address: Department of Physics, University of Ioannina, Ioannina 45110, Greece.
‡Present address: National Superconducting Cyclotron Laboratory and Department of Physics and Astronomy, Michigan State University, East Lansing, MI 48824.

especially for the mass-symmetric entrance channel [12].

In this paper, we present the results of a study on the decay of ^{160}Er* produced in the reactions ^{16}O + ^{144}Nd and ^{64}Ni + ^{96}Zr at the excitation energy of $E^* \approx 54$ MeV. As in Ref. [11], the observed γ-ray fold distributions of the xn products show differences depending on the entrance channel. For the description of the fusion process in these systems, we make use of a one-dimensional barrier penetration model with energy-dependent barriers as applied in Ref. [12] for the reactions ^{16}O + ^{148}Sm and ^{64}Ni + ^{100}Mo. It is shown that the model accounts well for the measured energy dependence of the average angular momentum in the ^{16}O + ^{144}Nd and ^{64}Ni + ^{96}Zr reactions [13,14]. Employing the appropriate σ_ℓ distributions in the statistical model results in a good description of all features of the ^{160}Er* decay observed in the present work.

While in this work we were able to explain the main features of the reactions, i.e., cross-section and γ-ray multiplicity distributions in terms of appropriate fusion models, the possibility of entrance-channel effects due to early reaction dynamics still remains. The formation time of the compound nucleus depends on the asymmetry of the entrance channel [15] which may lead to differences in the decay process. Such effects were reported by Thoennessen *et al.* [16] where a reduction in the γ-ray emission in the giant-dipole region was observed for the more symmetric fusion when ^{164}Yb was produced at 47 MeV of excitation by the ^{16}O + ^{148}Sm and ^{64}Ni + ^{100}Mo reactions. Since the early reaction dynamics is operating for a small fraction of the total reaction time and is affecting only the weak energetically expensive decay modes, it is not expected to alter significantly the main xn channel cross sections or their spin distributions in the fusion reactions that we address here.

II. EXPERIMENTAL PROCEDURES

Heavy-ion (HI) beams of ^{64}Ni ($E_{\rm lab} = 242.0$ MeV) and ^{16}O ($E_{\rm lab} = 87.0$ MeV), accelerated by the HHIRF Tandem, bombarded targets of ^{96}Zr and ^{144}Nd, respectively. Typical beam intensities measured at the Faraday cup were ~ 23 nA for ^{64}Ni and ~ 7.4 nA for ^{16}O. The targets consisted of highly enriched, self-supporting metallic foils of Zr (926 μg/cm^2, enriched to 85.25% in ^{96}Zr) and Nd (1360 μg/cm^2, enriched to 97.51% in ^{144}Nd). The beam energy loss through these targets was estimated to be $\sim$ 18.2 MeV (in ^{96}Zr) and $\sim$ 2.9 MeV (in ^{144}Nd), taking into account the 63.4° angle between the target surface and the beam. The average beam energies where the reactions took place were estimated to be very close to the beam energies in the middle of the targets: $\sim$ 235.0 MeV and $\sim$ 85.6 MeV, respectively. These estimates are based on the bombarding energy dependence of fusion cross sections known from reported evaporation residue excitation function measurements [13,14]. The initial excitation energies of the compound nucleus ^{160}Er* were calculated to be 54.5 MeV and 54.6 MeV in the ^{64}Ni- and ^{16}O-induced reactions, respectively.

Light charged particles (p, d, ^{3}He, α) emitted in these reactions were detected by the Dwarf Ball; a nearly 4π CsI(Tl) scintillator array [17], consisting of 70 equal solid angle detectors covering laboratory angles from $\theta_{\rm lab} = 12°$ to 168°. The energy calibration procedures were the same as in Ref. [11], where they are described in detail.

Residual nuclei were identified by their discrete γ-ray transitions, detected in an array of 18 Compton-suppressed Ge detectors inserted in the Oak Ridge Spin Spectrometer array [18]. The Ge array was always required to make an event trigger. Scaled-down events where the Ge detector was the trigger were stored in order to provide data for the (HI,xn) channels. The scale-down factor was adjusted in order to equalize approximately the rates of γ-particle coincidences and γ-ray singles stored during the data aquisition. The Ge detectors were calibrated for energy and efficiency using standard γ-ray sources of ^{152}Eu, ^{60}Co, ^{88}Y, ^{133}Ba, and ^{182}Ta.

The γ-ray multiplicity distributions for each identified exit channel were measured using 52 NaI(Tl) detectors of the Spin Spectrometer and the 18 anti-Compton shields of the Ge detector array. For the NaI(Tl) detectors of the Spin Spectrometer good separation between neutron and γ-ray pulses was achieved by time-of-flight techniques, using the average t_0 procedure described in Ref. [18]. For the anti-Compton shields, the limited timing resolution prevented the complete identification of neutron and γ-ray pulses. Energy and efficiency calibrations of the Spin Spectrometer detectors were obtained using γ-ray sources according to the procedures of Ref. [11]. The response functions of the Spin Spectrometer, providing the γ-ray multiplicity (M_γ) as a function of the γ-ray coincidence fold (k_γ), were obtained using data from the above sources in the equal energy approximation [18].

The experimental setup made possible the observation of the γ-ray fold distributions of channel-selected evaporation residues and the associated energy and angular distributions of the emitted charged particles. Absolute cross sections were measured by integrating the beam current and correcting for the average effective charges, $\bar{q}_{\rm Ni} = 21.47$ and $\bar{q}_{\rm O} = 7.24$, determined for equilibrated projectile charge states in their passage through the target. The maximum systematic error in the cross sections reported below is estimated to be $\simeq$ 17%. This error includes an estimated 3% error in the average projectile charge, 4% for the target thickness, 5% for the solid angle per detector, and 5% for the Ge detector efficiencies.

Table I lists the measured evaporation residue cross sections for the xn and αxn channels in the ^{64}Ni + ^{96}Zr and ^{16}O + ^{144}Nd reactions. These cross sections were obtained from the discrete γ-ray transitions given in Table I.

The measured angular and energy distributions of emitted protons and α particles were transformed event by event in the center-of-mass (c.m.) system assuming two-body kinematics. In both systems, the αxn cross sections were found to be small. For ^{64}Ni + ^{96}Zr, the angular distributions of the α particles associated with the αxn channels were found to be symmetric about 90° in the c.m. system. However, for ^{16}O + ^{144}Nd the angular distributions showed an excess of forward emitted α particles in the $\alpha 2n$ channel, a finding similar to the one

TABLE I. Identifying transitions and experimental cross sections of evaporation residues observed in the present work.

Residue	Channel	E_γ (keV)	Transition	Δk_γ [a]	$\sigma \pm \delta\sigma$ [b] (mb)	$\sigma \pm \delta\sigma$ [b] (mb)
					$^{16}O + {}^{144}Nd$	$^{64}Ni + {}^{96}Zr$
^{158}Er	$2n$	192.1	$2^+ \rightarrow 0^+$		6 ± 3	13 ± 3
^{157}Er	$3n$	266.4	$\frac{17}{2}^+ \rightarrow \frac{13}{2}^+$	2.75	165 ± 17	105 ± 10
^{156}Er	4n	344.6	$2^+ \rightarrow 0^+$		523 ± 50	113 ± 12
^{155}Er	$5n$	475.7	$\frac{17}{2}^+ \rightarrow \frac{13}{2}^+$	2.75	56 ± 6	$4.0^{+2.0}_{-4.0}$
^{154}Dy	$\alpha 2n$	334.5	$2^+ \rightarrow 0^+$		17 ± 2	4.9 ± 1.5
Total					767 ± 73	239 ± 16

[a]Shift applied in the corresponding fold distributions.
[b]Statistical error.

observed in the previously studied $^{16}O + {}^{148}Sm$ reaction [11]. A detailed analysis identified the origin of this component with an incomplete fusion process in which the ^{16}O projectile breaks up into $^{12}C + \alpha$, followed by fusion of ^{12}C with the target nucleus [11]. In the present work, we limit our discussion to the observables related to the most prominent xn decay channels.

Entry state distributions (in γ-ray fold and total γ-ray pulse height) of evaporation residues were extracted using the information provided by the Spin Spectrometer. The experimental k_γ distributions of the odd mass evaporation residues were shifted by Δk_γ in cases where the gating γ transition leads to a state of nonzero spin. The applied shifts are given in Table I. This correction accounts for the number of γ rays that would have been emitted if the ground state of the residual nucleus was zero or for those low-energy transitions which are below the energy threshold of the Spin Spectrometer (e.g., $^{157,155}Er$). It was assumed that $\Delta I = 2\Delta M_\gamma \approx 2\Delta k_\gamma$. This way, a direct comparison can be made between the experimental fold distributions and the calculated ones with the statistical model in which details of nuclear structure are ignored.

Figure 1 shows the experimental γ-ray fold distributions of various xn channels as a function of $k_{\text{eff}} = k_\gamma + \Delta k_\gamma$, for the two reactions. Apart from the difference in the absolute magnitude of the respective cross sections, we observe the following features of the distributions for $4n$ and $3n$ channels: The k_γ distributions in $^{64}Ni + {}^{96}Zr$ are broader than in $^{16}O + {}^{144}Nd$. Furthermore, the centroids in $^{64}Ni + {}^{96}Zr$ are displaced to a k_{eff} value higher than in $^{16}O + {}^{144}Nd$. More specifically, the centroid of the $3n$ channel shows a displacement from $k_{\text{eff}} = 20.0$ to 17.6 and the $4n$ channel a smaller displacement from 12.5 to 13.6. Due to low statistics, the k_γ distribution associated with the $2n$ channel in the $^{16}O + {}^{144}Nd$ reaction is not shown.

Another comparison can be made by constructing the cross section ratios $\sigma_i(k)/\Sigma\sigma_i(k)$, where the summation is taken over the xn channels which represent the bulk of the measured yields. These ratios are plotted in Fig. 2 as a function of k_{eff}, for the two reactions. In $^{16}O + {}^{144}Nd$, the ratios of the $3n$ and $4n$ channels cross at $k_{\text{eff}} = 18.5$, whereas in $^{64}Ni + {}^{96}Zr$ they cross at $k_{\text{eff}} = 17.5$. The above differences in the residual γ-ray fold distributions, namely, a broadening as well as a shift of the k_γ distributions for the reaction involving the nearly symmetric system, are similar to the one reported in Ref. [11].

It is of interest to investigate to what extent the above differences could indicate a possible dependence of the $^{160}Er^*$ decay on the formation mode. However, the independence of formation and decay of the compound nucleus has to be examined in terms of the compound nucleus spin. Such an investigation requires knowledge of the relation between the evaporation residue γ-ray fold distributions and the (primary) compound nucleus spin

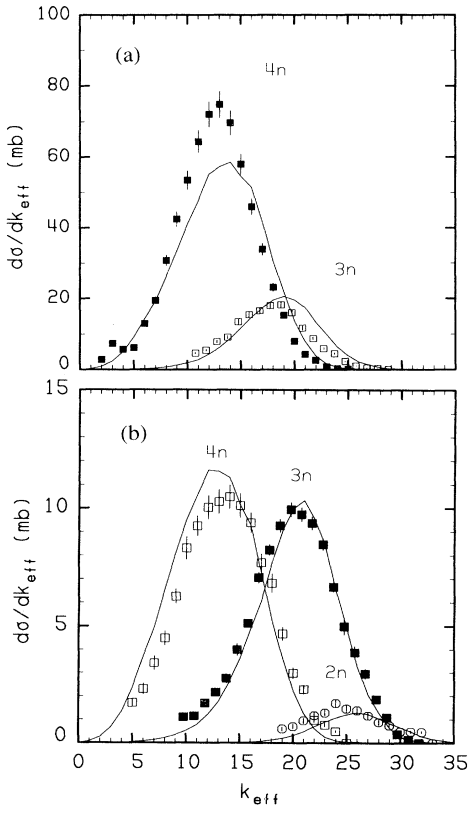

FIG. 1. (a) Experimental γ-ray fold distributions of the observed xn channels in 87 MeV $^{16}O + {}^{144}Nd$ reactions (symbols). The solid curves show the result of statistical model calculation described in the text. (b) Same as in (a), for 242 MeV $^{64}Ni + {}^{96}Zr$ reactions.

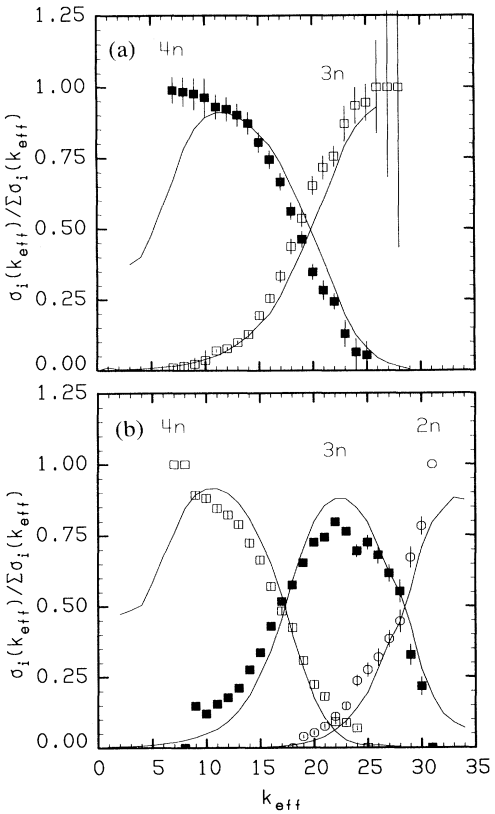

FIG. 2. Experimental (symbols) and calculated (solid lines) cross-section ratios $\sigma_i(k)/\Sigma\sigma_i(k)$ as a function of $k_{\rm eff}$, for the indicated xn channels in (a) ^{16}O + ^{144}Nd and (b) ^{64}Ni + ^{96}Zr reactions.

distribution. This correspondence is obtained via the statistical model. Two different approaches have previously been used for the comparison of the two reactions. In a first approach, one may attempt to deduce the compound nucleus spin distribution from the residue k_γ distributions. This procedure was followed in Ref. [10] using techniques similar to those developed in Refs. [19–21]. This involves retrieving the compound nucleus angular momentum distribution by transforming from k_γ to γ-ray multiplicity (M_γ), then to the entry state spin, and finally to the compound nucleus spin. However, it has to be noted that the techniques of Refs. [19–21] are best suited for the transformation of distribution *averages* and not for *distributions*. More recently, a more refined event-by-event unfolding method was reported in Ref. [22].

To avoid problems with consecutive unfoldings, which may not give unique solutions in the case of tails of distributions, we have opted for the following approach [11]. Through the use of a fusion model we produce compound nucleus spin distributions (σ_ℓ) with parameters adjusted to fit measured fusion excitation functions for both reactions [13,14]. In the subsequent statistical model calculations, the entry-state (E^*, I), and the (E^*, M_γ) distributions of each residue are obtained. By folding the (E^*, M_γ) distributions with the measured $(E^*, M_\gamma) \rightarrow (H_\gamma, k_\gamma)$ responses of the Spin Spectrometer, we obtain by projection the theoretical k_γ distributions which can be compared directly with the experimental ones.

III. MODEL CALCULATIONS

A. Fusion process

The symbols in Fig. 3 show the measured total evaporation residue cross sections and average angular momenta as a function of the center-of-mass energy, for ^{16}O + ^{144}Nd. Open and solid circles refer to the measurements of Ref. [13] and the open square to the present work. In Fig. 4, similar measurements for ^{64}Ni + ^{96}Zr are shown, where the solid circles stand for the results of Ref. [14] and the open square for the present work.

The dashed curves in Figs. 3 and 4 show the predictions of a one-dimensional barrier penetration calculation for these systems. This calculation makes use of the Akyüz and Winther potential [23] with nuclear potential strength adjustments as in the previously studied ^{16}O + ^{148}Sm and ^{64}Ni + ^{100}Mo reactions [12]. For ^{16}O + ^{144}Nd, the fusion cross sections are described reasonably well in the near-barrier region and overestimated slightly at higher energies [Fig. 3(a)]. However, the low-energy

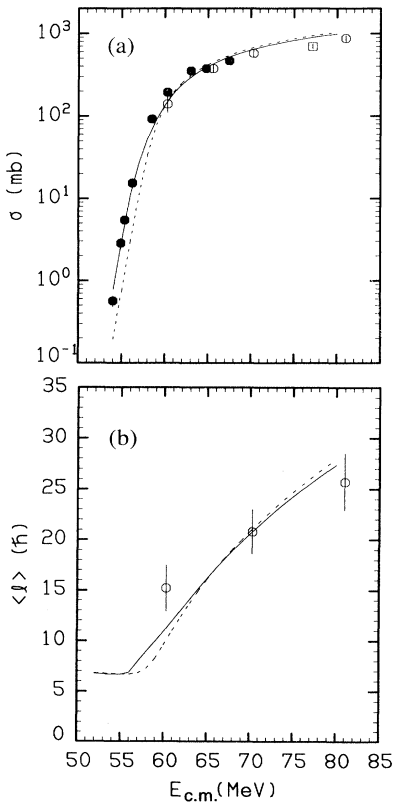

FIG. 3. Fusion cross sections and mean angular momenta versus $E_{\rm c.m.}$ in ^{16}O + ^{144}Nd reactions (symbols). The dashed and solid curves show the calculations with the one-dimensional and the energy-dependent barrier penetration models, respectively.

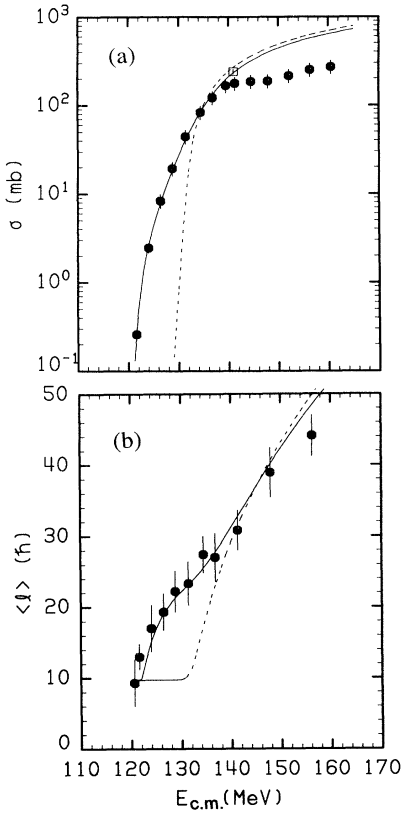

FIG. 4. Fusion cross sections and mean angular momenta versus $E_{\text{c.m.}}$ in ^{64}Ni + ^{96}Zr reactions (symbols). The dashed and solid curves show the calculations with the one-dimensional and the energy-dependent barrier penetration models, respectively.

cross-section measurements are systematically underpredicted. A similar trend is observed in the description of the measured $\langle \ell \rangle$ [Fig. 3(b)], where the calculation describes well the medium energy datum, but tends to overpredict (and underpredict) the high- (and low-) energy measurements. The calculation for ^{64}Ni + ^{96}Zr [Fig. 4(a)] reproduces the magnitude of the fusion cross sections only in the energy region around $E_{\text{c.m.}} \approx 137$ MeV. At higher energies, the experimental data are overestimated. In the low-energy region, the model strongly underpredicts the measured cross sections by more than two orders of magnitude. Again, we observe a similar trend in the description of $\langle \ell \rangle$, namely, a strong underprediction of the low-energy data, a good description in the medium-energy region, and an overprediction of the highest energy measurement [Fig. 4(b)]. At high energies, the disagreement between the data and the model predictions can be understood in terms of the onset of fission competition in this nearly symmetric reaction [14] given the fact that the data correspond to the sum of the evaporation residues. In both reactions, the underestimation of σ_{fus} and $\langle \ell \rangle$ at low energies shows the inadequacy of the one-dimensional barrier penetration model in the description of the fusion process [1,2].

Several theoretical approaches developed for the description of subbarrier σ_{fus} and $\langle \ell \rangle$ data are reviewed in Refs. [1,2]. In Ref. [24], the subbarrier fusion process was examined from the point of view of a macroscopic model of nuclear shape evolution [25]. It was suggested that the fusing system samples an energy-dependent effective barrier which coincides with the one-dimensional sudden potential barrier at bombarding energies near and above it, while it coincides with the adiabatic potential barrier at bombarding energies much below. At intermediate bombarding energies, a smooth transition of the effective barrier is expected to take place from the sudden to the adiabatic barrier. The sudden potential barrier is associated with the one extracted from frozen density potentials, whereas the adiabatic potential barrier corresponds to the completely relaxed configuration. A simple inversion method was followed to extract the effective fusion barriers from fusion excitation function data [24]. This procedure makes use of the expression for the fusion cross section,

$$\sigma_{\text{fus}}(E) = \pi \lambda \int (2\ell + 1) T_\ell(E) d\ell, \tag{1}$$

where k is the asymptotic wavelength in the entrance channel and

$$T_\ell(E) = T_0 \left[E - \frac{\ell(\ell+1)\hbar^2}{2\mu R^2} \right] \tag{2}$$

is the transmission coefficient for fusion. In Eq. (2), it is assumed that the barrier increases with ℓ by the addition of the centrifugal term $\ell(\ell+1)\hbar^2/2\mu R^2$. One obtains

$$\sigma_{\text{fus}}(E) = \frac{\pi R^2}{E} \int T_0(E') dE'. \tag{3}$$

Therefore

$$\frac{d}{dE} \left| \frac{E\sigma}{\pi R^2} \right| = T_0(E). \tag{4}$$

Using the parabolic approximation of the fusion barrier,

$$T_0(E) = \{1 + \exp[2\pi(B_{\text{eff}} - E)/\hbar\omega]\}^{-1}, \tag{5}$$

whence

TABLE II. Barrier penetration parameters.

System	V_b[a] (MeV)	R_b[a] (fm)	$\hbar\omega$[a] (MeV)	V_1 (MeV)	V_2 (MeV)	E_1 (MeV)	E_2 (MeV)
^{16}O + ^{144}Nd	58.00	11.19	4.44	57.00	65.72	55.75	73.94
^{64}Ni + ^{96}Zr	131.67	11.40	3.48	123.99	150.00	121.89	154.02

[a] s-wave values.

$$B_{\text{eff}} = E + (\hbar\omega/2\pi)\ln[1 - T_0(E)]/T_0(E). \quad (6)$$

Once R and $\hbar\omega$ are specified, the effective barrier height B_{eff} can be determined from the experimental data. In the analysis of Ref. [24], R was treated as energy independent and equal to the fusion barrier radius R_b implied by the near-barrier data. The barrier curvature $\hbar\omega$ was determined from the extreme subbarrier data. It was shown that the extracted barriers exhibit the energy dependence suggested by the macroscopic model. A systematic analysis of fusion excitation functions [26] was also found consistent with these observations.

For the purpose of creating spin distributions for the systems of the present study, we adopted the procedure of Refs. [24–27]. An energy-dependent fusion barrier,

$$V_b(\epsilon) = \begin{cases} V_2 & \text{for } \epsilon > E_2, \\ V_1 + \frac{V_2 - V_1}{E_2 - E_1}(\epsilon - E_1) & \text{for } E_1 < \epsilon < E_2, \\ V_1 & \text{for } \epsilon < E_1, \end{cases} \quad (7)$$

was introduced in the one-dimensional barrier penetration model [12]. In our calculations, the angular momentum dependence of the fusion barrier radii R_b and barrier curvatures $\hbar\omega$ was taken into account with nuclear potential parameters that describe closely the near-barrier data. V_1, V_2, E_1, and E_2 were treated as free parameters (see Table II) to fit the fusion excitation functions in an iterative procedure. The resulting fits of the fusion excitation functions and the deduced bombarding energy dependence of the $\langle\ell\rangle$ are shown with the solid lines in Figs. 3 and 4. It is realized that the energy-dependent barrier penetration model provides a good description of the $\langle\ell\rangle$ data, especially for the ^{64}Ni + ^{96}Zr reaction.

B. Compound nucleus decay

The decay of ^{160}Er* produced in the two reactions was described with the statistical model making use of the spin distributions produced with the energy-dependent barrier penetration model. The statistical model calculations were carried out with the code EVAP [28]. The level density formalism of Gilbert and Cameron [29] was employed with a level density parameter of $a = A/8.5$ MeV^{-1}. Penetrabilities for particle emission were calculated from the optical model using the global parametrizations of Wilmore and Hodgson [30], Perey [31], and McFadden and Satchler [32] for neutron, proton, and alpha particles, respectively. In the description of γ competition, emission of $E1$, statistical and collective $E2$, $M1$, and $M2$ γ rays was included. The $E1$ γ-ray emission strength function included the giant dipole resonance (GDR) with shape and position taken from systematics [33,34] and strength determined by the classical energy-weighted sum rule [34]. The admixture of exchange forces in the nuclear force was assumed to be 50%. The GDR splitting due to deformation was included using a double-Lorentzian GDR shape corresponding to an input prolate deformation parameter β_{GDR}=0.2. The γ strengths for $M1$, statistical $E2$, $E2_{\text{coll}}$, and $M2$ were set equal to 0.01, 10.0, 100.0, and 1.2 W.u., respectively. The above parameter set is the same as the one used in the description of ^{170}Yb* decay [12].

For ^{16}O + ^{144}Nd, evaporation calculations were performed at a beam energy corresponding to the one in the middle of the target. This is justified by the fact that the fusion cross section in the energy region of interest is not steeply rising. By folding the calculated (E^*, M_γ) distributions with the measured $(E^*, M_\gamma) \rightarrow (H_\gamma, k_\gamma)$ responses of the Spin Spectrometer, we obtain by projection the theoretical k_γ distributions to be compared with the data. The comparison of the experimental and calculated distributions for the $3n$ and $4n$ channels is made in Fig. 1. The overall agreement is reasonably good despite a tendency of the calculation to overestimate the peak position of the distributions. This can be explained by the fact that the calculated fusion excitation function at the energy of the present study overestimates the measured cross section [Fig. 3], thus allowing for an excess of high-ℓ partial waves.

For ^{64}Ni + ^{96}Zr, detailed statistical model calculations were performed in order to take into account the energy loss of the beam through the target in connection with the steepness of the fusion excitation function [Fig. 4(a)]. The target was divided into a number of slices, each representing a 1 MeV energy drop of the beam in the laboratory system. Statistical model calculations were performed at the beam energy in the middle of each slice. In each case, the k_γ distributions of the xn products were deduced. The results of these calculations were averaged and compared with the experimental data. In Fig. 1(b) we show the comparison between the experimental and calculated k_γ distributions of the $2n$, $3n$, and $4n$ channels in the ^{64}Ni + ^{96}Zr reaction. The overall agreement is good.

The calculated cross section ratios $\sigma_i(k)/\Sigma\sigma_i(k)$ as a function of k_{eff} are shown by the solid lines in Fig. 2, where they are compared with the data. The calculation provides a good description of the data for both reactions. The underprediction of the $4n$ ratio below $k_{\text{eff}} \approx 10$, for ^{16}O + ^{144}Nd, is due to the fact that the statistical model predicts the existence of a cross section for the $5n$ channel for which the k_{eff} distribution was not extracted. However, 56 mb for the $5n$ channel was observed with poorly defined k_{eff} values between 2 and 8, compared to 523 mb for the $4n$ channel. This would improve the agreement with the calculation below $k_{\text{eff}} \sim 10$.

IV. DISCUSSION

In the present work, the γ-ray fold distributions of residual nuclei resulting from ^{160}Er*(54 MeV) after neutron evaporation were studied. The role of entrance-channel mass asymmetry in the compound nucleus decay was tested in the study of the reactions ^{16}O + ^{144}Nd and ^{64}Ni + ^{96}Zr producing ^{160}Er* at the same excitation energy.

For the description of the fusion process a one-dimensional barrier penetration model with energy-dependent fusion barriers was adopted. Despite the simplicity of the model, a good description of the bombarding energy dependence of measured average angular mo-

menta for ^{64}Ni + ^{96}Zr was obtained. For ^{16}O + ^{144}Nd, the degree of agreement with the data was found reasonably good, similar to the one reported in Ref. [13], where the data were compared with simplified coupled-channels calculations. Parameters extracted by fitting fusion excitation functions of the above reactions were used in predicting the shapes of the σ_ℓ distributions under the bombarding conditions of the present experiment. These distributions were found sufficient to describe well most of the experimental data of the present work. On the basis of the above findings it is realized that the ^{160}Er* decay at $E^* \approx 54$ MeV can be described well in terms of the statistical model taking into account spin distributions which describe consistently the corresponding fusion excitation function data. This corroborates earlier results of a similar study of the ^{164}Yb* decay in the ^{16}O + ^{148}Sm and ^{64}Ni + ^{100}Mo of Barreto *et al.* [11]. It has to be pointed out that the degree of agreement of the statistical model calculations with the data for the nearly symmetric system in the present study appears to be superior to the corresponding one of Ref. [11].

According to the model predictions, under the bombarding energy conditions of the present study, the unitarity limit is not fully exhausted for ^{64}Ni + ^{96}Zr (see Fig. 5). This is only in qualitative agreement with the results of Kühn *et al.* [7] on the same reaction under similar bombarding conditions. In the work of Kühn *et al.*, the shape of the experimentally extracted σ_ℓ distribution suggests a much stronger reduction (cf. Fig. 1 of Ref. [7]). However, it has to be noted that the absolute normalization was obtained from a different experiment [5]. The recent cross-section measurements of ^{64}Ni on ^{92,96}Zr of Stefanini *et al.* [14] establish a cross section which is 25% higher than the one of Ref. [5]. Therefore, the above discrepancy can be attributed to systematic errors in the cross section measurements. We believe that simultaneous cross section and spin distribution measurements are needed in order to ascertain the low-spin behavior of the σ_ℓ distributions.

In summary, we have observed apparent entrance channel effects in the spin distributions in evaporation residue cross sections in the reactions ^{16}O + ^{144}Nd and ^{64}Ni + ^{96}Zr producing ^{160}Er* at the same excitation energy, that are similar to previous observations. The difference between the present work and earlier similar studies, e.g., Ref. [10], is that when realistic fusion models are used in the calculation of the input σ_ℓ distributions, then statistical model simulations that incorporate the detector responses reproduce satisfactorily the data. In these calculations the more symmetric fusion leads to very extended ℓ distributions that play a crucial role in determining the observed differences. Thus we find no need to resort to strong structural influences on the de-excitation of the compound nucleus. As in the work of Barreto *et al.* [11] the αxn channels are influenced by incomplete fusion processes that explain the observed differences. Finally, we point out that entrance channel effects in the early fusion dynamics [15] are important here. This is because reactions with different mass asymmetry can lead to differences in the early stages of the decay process. Sensitive probes, such as the γ−ray emission in the giant resonance region, are needed in this case to observe the differences [16]. It would be of great interest to find additional probes for these early dynamics effects.

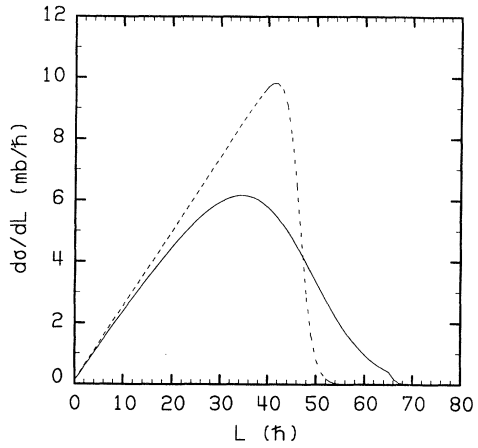

FIG. 5. Spin distribution for $E_{c.m.} = 141$ MeV ^{64}Ni + ^{96}Zr according to the one-dimensional (dashed curve) and the energy-dependent barrier penetration models (solid curve).

ACKNOWLEDGMENTS

J.L.B. acknowledges travel support from CNPq-Brazil, and Lafex-CBPF for use of its computer facilities for part of this work. This work was supported by the Director, Office of Energy Research, Office of High Energy and Nuclear Physics, Nuclear Physics Division of the U.S. Department of Energy, under Grants Nos. DE-FG02-88-ER40406 and DE-FG02-87-ER40316. Oak Ridge National Laboratory is managed by Martin Marietta Energy System, Inc. under Contract No. DE-AC05-84OR21400 with the Department of Energy.

[1] M. Beckerman, Rep. Prog. Phys. **51**, 1047 (1988).
[2] R. Vandenbosch, Annu. Rev. Nucl. Part. Sci. **42**, 447 (1992).
[3] D.E. DiGregorio and R.G. Stokstad, Phys. Rev. C **43**, 265 (1991).
[4] A. Charlop, J. Bierman, Z. Drebi, A. Garcia, D. Prindle, A.A. Sonzogni, R. Vandenbosch, D. Ye, S. Gil, F. Hasenbalg, J.E. Testoni, D. Abriola, M. di Tada, A. Etchegoyen, M.C. Berisso, J.O. Fernandez-Niello, and A.J. Pacheco, Phys. Rev. C **49**, R1235 (1994).
[5] B. Haas, G. Duchène, F.A. Beck, T. Byrski, C. Gehringer, J.C. Merdinger, A. Nourredine, V. Rauch, J.P. Vivien, J. Barrette, S. Tobbeche, E. Bożek, J. Styczen, J. Keinonen, J. Dudek, and W. Nazarewicz, Phys.

Rev. Lett. **54**, 398 (1985).
[6] C.H. Dasso and S. Landowne, Phys. Rev. C **32**, 1094 (1985).
[7] W. Kühn, A. Ruckelshausen, R.D. Fischer, G. Breitbach, H.J. Hennrich, V. Metag, R. Novotny, R.V.F. Janssens, T.L. Khoo, D. Habs, D. Schwalm, B. Haas, and R.S. Simon, Phys. Rev. Lett. **62**, 1103 (1989).
[8] W. Kühn, P. Chowdhury, R.V.F. Janssens, T.L. Khoo, F. Haas, J. Kasagi, and R.M. Ronningen, Phys. Rev. Lett. **51**, 1858 (1983).
[9] D.J. Love, P.J. Bishop, A. Kirwan, P.J. Nolan, D.J. Thornley, A.H. Nelson, and P.J. Twin, Phys. Rev. Lett. **57**, 551 (1986).
[10] A. Ruckelshausen, R.D. Fischer, W. Kühn, V. Metag, R. Mühlhans, R. Novotny, T.L. Khoo, R.V.F. Janssens, H. Gröger, D. Habs, H.W. Heyng, R. Repnow, D. Schwalm, G. Duchène, R.M. Freeman, B. Haas, F. Haas, S. Hlavac, and R.S. Simon, Phys. Rev. Lett. **56**, 2356 (1986).
[11] J.L. Barreto, N.G. Nicolis, D.G. Sarantites, R.J. Charity, L.G. Sobotka, D.W. Stracener, D.C. Hensley, J.R. Beene, C. Baktash, M. Halbert, and M. Thoennessen, Phys. Rev. C **48**, 2881 (1993).
[12] N.G. Nicolis and D.G. Sarantites, Phys. Rev. C **48**, 2895 (1993).
[13] G. Duchène, P. Romain, F.A. Beck, Ph. Benet, D. Disdier, B. Haas, B. Lott, V. Rauch, F. Scheibling, J.P. Vivien, S.K. Basu, E. Bożek, K. Zuber, D. DiGregorio, and J. Fernandez-Niello, Phys. Rev. C **47**, 2043 (1993).
[14] A.M. Stefanini, L. Corradi, D. Ackermann, A. Facco, F. Gramegna, H. Moreno, L. Mueller, D.R. Napoli, G.F. Prete, P. Spolaore, S. Beghini, G. Montagnoli, G. Nebbia, J.A. Ruiz, G.F. Segato, C. Signorini, and G. Viesti, Nucl. Phys. **A548**, 453 (1992).
[15] H. Feldmeier, Rep. Prog. Phys. **50**, 915 (1987).
[16] M. Thoennessen, J.R. Beene, F.E. Bertrand, C. Baktash, M.L. Halbert, D.J. Horen, D.G. Sarantites, W. Spang, and D.W. Stracener, Phys. Rev. Lett. **70**, 4055 (1993).
[17] D.W. Stracener, D.G. Sarantites, L.G. Sobotka, J. Elson, J.T. Hood, Z. Majka, V. Abenante, A. Chbihi, and D.C. Hensley, Nucl. Instrum. Methods A **294**, 485 (1990).
[18] M. Jääskeläinen, D.G. Sarantites, R. Woodward, F.A. Dilmanian, J.T. Hood, R. Jääskeläinen, D.C. Hensley, M. Halbert, and J.H. Barker, Nucl. Instrum. Methods **204**, 385 (1983).
[19] D.G. Sarantites, L. Westerberg, M.L. Halbert, R.A. Dayras, D.C. Hensley, and J.H. Barker, Phys. Rev. C **18**, 774 (1978).
[20] L. Westerberg, D.G. Sarantites, D.C. Hensley, R.A. Dayras, M.L. Halbert, and J.H. Barker, Phys. Rev. C **18**, 796 (1978).
[21] R.A. Dayras, R.G. Stokstad, C.B. Fulmer, D.C. Hensley, M.L. Halbert, R.L. Robinson, A.H. Snell, D.G. Sarantites, L. Westerberg, and J.H. Barker, Phys. Rev. Lett. **42**, 697 (1979).
[22] M.L. Halbert and J.R. Beene, in *Proceedings of the XIV Symposium on Nuclear Physics,* Cuernavaca, Mexico, 1991, edited by M.E. Brandan (World Scientific, Singapore, 1991).
[23] Ö. Akyüz and A. Winther, in *Proceedings of the Enrico Fermi International School of Physics*, 1979, edited by R.A. Broglia, C.H. Dasso, and R. Ricci (North-Holland, Amsterdam, 1981), p. 492.
[24] V.S. Ramamurthy, A.K. Mohanty, S.K. Kataria, and G. Rangarajan, Phys. Rev. C **41**, 2702 (1990).
[25] W.J. Swiatecki, Phys. Scr. **24**, 113 (1981).
[26] A.K. Mohanty, S.V.S. Sastry, S.K. Kataria, and V.S. Ramamurthy, Phys. Rev. C **46**, 2012 (1992).
[27] A.K. Mohanty, S.V.S. Sastry, S.K. Kataria, and V.S. Ramamurthy, Phys. Rev. Lett. **65**, 1096 (1990).
[28] N.G. Nicolis, D.G. Sarantites, and J.R. Beene, computer code EVAP (unpublished); evolved from the code PACE by A. Gavron, Phys. Rev. C **21**, 230 (1980).
[29] A. Gilbert and A.G.W. Cameron, Can. J. Phys. **43**, 1446 (1965).
[30] D. Wilmore and P.E. Hodgson, Nucl. Phys. **55**, 673 (1964).
[31] F.G. Perey, Phys. Rev. **131**, 745 (1963).
[32] L. McFadden and G.R. Satchler, Nucl. Phys. **84**, 177 (1966).
[33] A. Bohr and B.R. Mottelson, *Nuclear Structure* (Benjamin, Reading, MA, 1975), Vol. II.
[34] S.S. Hanna, in *Giant Multipole Resonances*, edited by F. Bertrand (Harwood, New York, 1980), Table I.